Journal of the European Ceramic Society 20 (2000) 1459–1468

# Pressureless sintering of $Al_2O_3$ containing up to 20 vol% zirconium diboride ($ZrB_2$)

Stefan Postrach *, Jürgen Pötschke

*Deutsches Institut für Feuerfest und Keramik GmbH, An der Elisabethkirche 27, D-53113 Bonn, Germany*

Received 5 August 1999; accepted 4 November 1999

**Abstract**

The production of particle composites by means of pressureless sintering provides a cost-effective alternative to production variants such as hot-pressing. However, minimal quantities of additives are sufficient to impede the densification of oxidic matrix components. This paper examines the sintering behaviour of alumina powder as a function of the volume fraction of $ZrB_2$ (up to 20 vol%). A distinction can be made between two sintering ranges according to the temperature: at $T \leqslant 1700^\circ$ a solid-state process applies. This process is decisively influenced by the boron oxide ($B_2O_3$) contained in the raw material $ZrB_2$. The validity of the Lange model, which describes the influence of increasing volumes of inclusions on the densification behaviour of a crystalline matrix phase, is confirmed in this temperature range. At $T > 1700^\circ$C, an aluminium borate melt occurs, accelerating the sintering process substantially. As a result, the composites quickly attain matrix densities greater than 95% of the theoretical density. At higher firing temperatures the $ZrB_2$ particles coalesce, resulting in the formation of an electrically conductive penetration structure at a content level of 20 vol%. 

*Keywords:* $Al_2O_3$; Inclusions; Microstructure-final; Sintering; $ZrB_2$

## 1. Introduction

The development of particle composites is an established method of optimising the properties of ceramic materials. It also enables the use of components which are economically unviable in a single-phase configuration on account of the high price of their raw materials and their poor densification properties. The production of composite materials proves problematic in many instances, however, as minimal additions of a second phase are sufficient to reduce the sintering activity of an oxidic matrix phase considerably.[1] Consequently, such materials are generally produced by hot-pressing. New, more cost-effective production processes need to be developed, in order to exploit the performance capabilities of these materials to the full.

One technically interesting combination is alumina ($Al_2O_3$) with a zirconium diboride ($ZrB_2$) addition. $ZrB_2$ is a hard material whose special properties include a high heat conductivity and high hardness.[2]

This paper establishes how various constituents of $ZrB_2$ (up to 20 vol%) affect the densification behaviour of the $Al_2O_3$ matrix under pressureless sintering conditions. The processes which occur and the ultimately produced microstructure are investigated with the aim of developing a ceramic material which possesses great practical potential as refractory material and metallic resistance material and is also viable from an economical point of view.

## 2. Experimental procedure

The employed raw material for the matrix is $Al_2O_3$ from the Martinswerke company, Germany (quality CS 400M). According to the manufacturer's information, the $Al_2O_3$ content is approx. 99.8% by weight. The average particle size is between 0.6 and 0.7 μm. The $ZrB_2$ (Elektroschmelzwerke Kempten, Deutschland) content is >94% by weight. According to the manufacturer's information, the main impurities are C, $O_2$ and $B_2O_3$. The average particle size is 7 μm.

The percentage volumes of 2.5, 5, 10 and 20% $ZrB_2$ relate to a dense material, and thus do not take account

* Corresponding author at new address: Schott Glaswerke, Hattenbergstr. 10, D-55014 Mainz, Germany.

*E-mail address:* difk-bonn@t-online.de (S. Postrach).

0955-2219/00/$ - see front matter 
PII: S0955-2219(00)00026-1

of the residual porosity. The respective percentages of $ZrB_2$ by weight are calculated in accordance with Eq. (1):

$$\text{weight\%}\,ZrB_2 = \frac{v_{ZrB_2} \cdot \rho_{ZrB_2}}{v_{ZrB_2} \cdot \rho_{ZrB_2} + v_{Al_2O_3} \cdot \rho_{Al_2O_3}} 100\% \qquad (1)$$

whereby

$v_{ZrB_2} = ZrB_2$ percentage by volume
$\rho_{ZrB_2}$ = density of $ZrB_2 = 6.1$ g/cm$^3$
$v_{Al_2O_3} = Al_2O_3$ percentage by volume
$\rho_{Al_2O_3}$ = density of $Al_2O_3 = 3.95$ g/cm$^3$.

The batches are homogenised for 5 h in a polyethylene container inside a tumbling mixer, adding methanol and $Al_2O_3$ balls, after which they are dried at 110°C. Powder compacts are produced (diameter: 20 mm; height: 10 mm). Therefore the mixtures are first subjected to uniaxial pressing, followed by final compression in a cold isostatic press at a pressure of 150 MPa.

The specimens are fired at various temperatures (1200–1900°C) in a graphite resistance furnace (Typ Astro, Thermal Technologies) under an argon (quality 4.8) gas flow at atmospheric pressure. The heating rate is 10 K/min.

After firing, the density of the specimens is determined in accordance with EN 993-1 by means of the water absorption method. The phase composition of selected specimens is determined with an X-ray diffractometer (Siemens D 500). The microstructure is also examined on polished sections from selected specimens by means of optic microscope and using a scanning electron microscope (Cambridge Stereoscan 250 Mk 2). For this purpose, the specimens are infiltrated with resin in vacuum. An electron beam microprobe (make: Cameca; model: Camebay) is also available, enabling a wavelength-dispersive X-ray detector to be used to determine the distribution of elements (qualitative, up to and including boron) in the micro range. The microstructure is also examined with a transmission electron microscope (TEM). The electrical conductivity is determined at room temperature, using the impedance principle. For this purpose, the end faces of the cylindrical specimens are ground plane-parallel and a coating of platinum is applied by means of vapour deposition in order to attain enhanced contact.

## 3. Results

### 3.1. Sintering process

Fig. 1 shows the relative density (as a percentage of the corresponding theoretical density) of $Al_2O_3$ containing various levels of $ZrB_2$ (2.5, 5, 10 and 20 vol%) as a function of the firing temperature. It is noticeable that the levels of $ZrB_2$ content as low as 2.5 vol% have very negative effects on relative density at temperatures up to 1700°C, while above 1700°C the negative influence clearly diminishes. On the contrary the additives increase the rate of sintering. X-ray diffraction analysis fails to detect the formation of a new phase in any of the specimens.

Two clear temperature ranges of different sintering kinetics thus apply. This is manifested by the corresponding densification rates of the matrix, which are determined as follows.

First of all, the matrix density is calculated:[3]

$$\rho_{mc} = \frac{\rho_C(\rho_{C0} - \rho_S f_0)}{\rho_{C0} - f_0 \rho_C} \qquad (2)$$

whereby

$\rho_{mc}$ = matrix density of composite in g/cm$^3$
$\rho_{C0}$ = green density of composite in g/cm$^3$
$\rho_C$ = density of composite in g/cm$^3$
$f_0$ = volume percentage of inclusion in green state ($ZrB_2$)
$\rho_s$ = theoretical density of inclusion ($ZrB_2$) = 6.1 g/cm$^3$

The courses of the relative matrix densities in the two temperature ranges are then approximated via separate curves (Fig. 2).

The sintering rate $\dot{\varepsilon}_m$ is then calculated as follows:

$$\dot{\varepsilon}_m = \frac{1}{\rho_{mc}} \frac{d\rho}{dT} \frac{dT}{dt}, \qquad (3)$$

whereby $dT/dt = 10$ K/min.

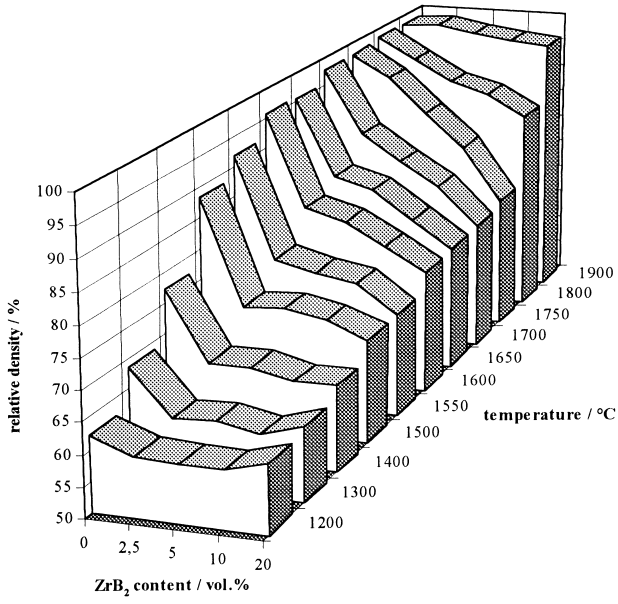


Fig. 1. Relative density of $Al_2O_3$ containing various levels of $ZrB_2$ as a function of the firing temperature (heating rate: 10 K/min; no soaking time; atmosphere: argon).

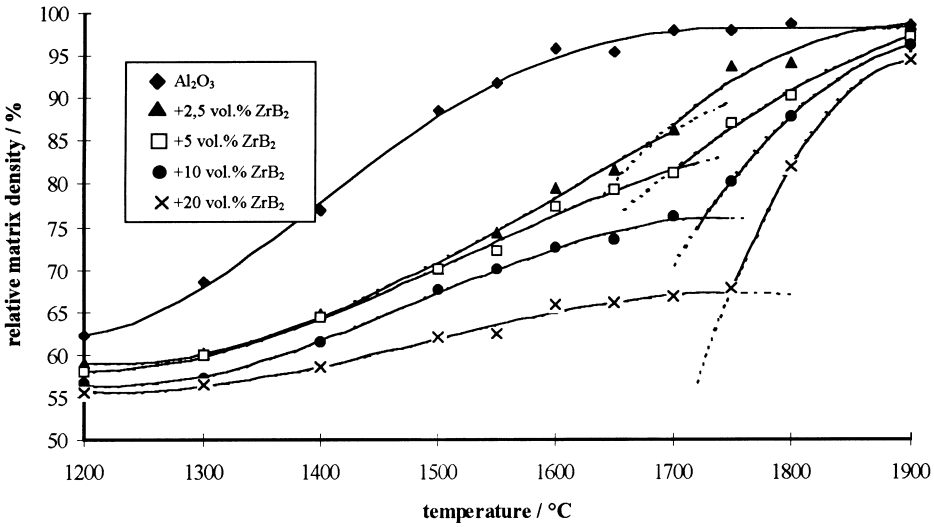


Fig. 2. Relative matrix density as a function of temperature for $Al_2O_3$ containing different levels of $ZrB_2$.

Fig. 3 shows that the added $ZrB_2$ initially results in a substantial reduction in the sintering rate. The sintering rates of all four composites drop slightly after attaining a maximum between 1450 and 1550°C. At temperatures >1700°C the sintering rate rapidly increases in all four cases, whereby increasing the $ZrB_2$ content levels lead to higher rates, as a result of which the final density of all specimens is approximately the same (cf. Fig. 2). The sintering rate of the specimen containing 20 vol% $ZrB_2$ give rise to a highest rate.

The influence of the soaking time on the relative matrix density of the composites at 1800°C is shown in Fig. 4. Within 60 min the relative matrix densities achieve values greater 95%.

### 3.2. Microstructure of composites containing 20 vol% $ZrB_2$

Fig. 5a shows the microstructure of the specimen containing 20 vol% $ZrB_2$ after firing for 1 h at 1600°C. The microstructure is very porous. The light-coloured sharp-edged phases are $ZrB_2$. The microstructure after firing for 1 h at 1800°C is clearly different (Fig. 5b): it is very dense, and contains small, closed pores of a maximum of 10 μm in diameter. The $ZrB_2$ particles, which are generally entirely enclosed by the matrix, have become markedly rounded and 'flow' together wherever they come into close proximity to one another. In this case the $ZrB_2$ particles are so strongly cross-linked that a penetration structure applies.

In isolated instances there are regions around the $ZrB_2$ particles which indicate a melt phase. Here, the melt has penetrated into the $Al_2O_3$ grain boundaries (Fig. 6a). Investigation of these regions with the microprobe reveals this to be a melt phase from the Al–B–O system. Pure $ZrB_2$ does not reveal any signs of sintering under the same conditions (Fig. 6b).

The TEM images for the specimen containing 20 vol% $ZrB_2$ sintered at 1800°C for 1 h reveal a sharp phase boundary between $Al_2O_3$ and $ZrB_2$. The rounding

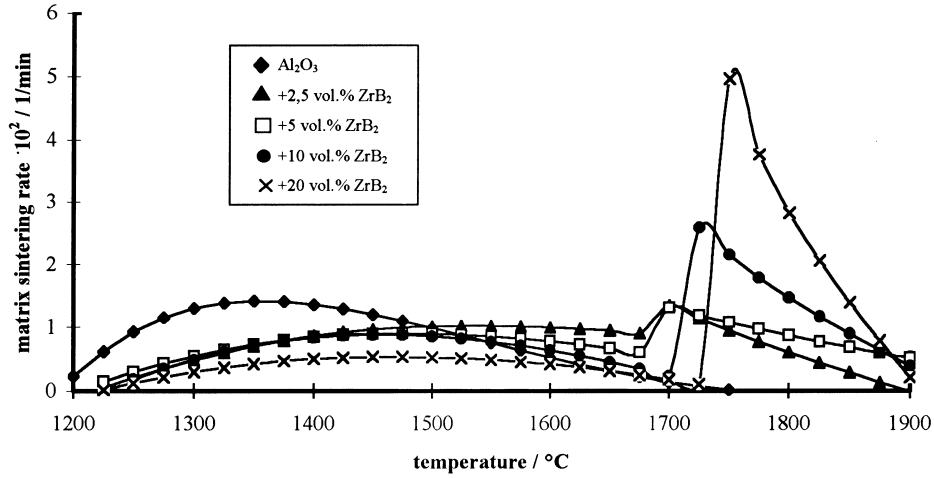


Fig. 3. Matrix sintering rate as a function of temperature for $Al_2O_3$ containing different levels of $ZrB_2$.

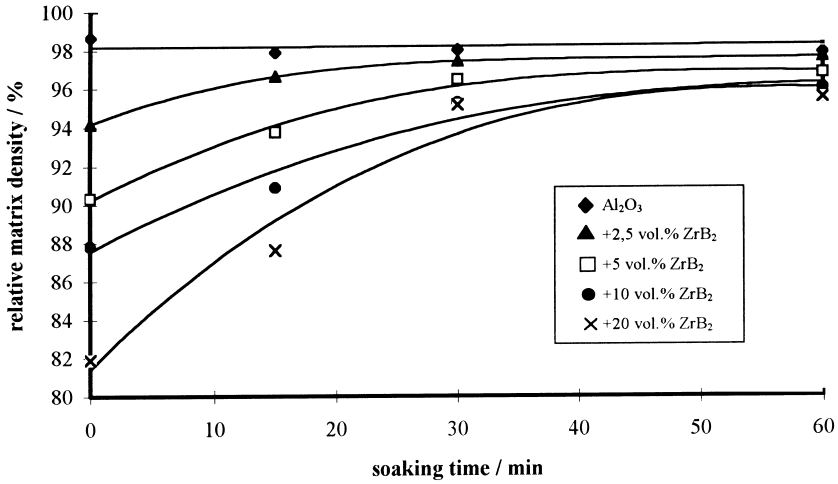


Fig. 4. Relative matrix density as a function of the soaking time at 1800°C.

of the $ZrB_2$ particles, which is clearly visible under the light microscope, results from a sawtooth-like arrangement of crystal faces (Fig. 7). An amorphous phase of approx. 0.1 μm in thickness develops in the pores on both the $Al_2O_3$ and the $ZrB_2$ surfaces, indicating the formation of a melt phase. Grain boundaries are visible where two or more $ZrB_2$ particles coalesce.

### 3.3. The influence of boron III oxide ($B_2O_3$) on the sintering behaviour of $Al_2O_3$

The main impurity in the $ZrB_2$ raw material is $B_2O_3$. It is thus appropriate to investigate the influence of minimal additions of this component on the sintering behaviour of $Al_2O_3$. The specimens are produced by first of all dissolving an appropriate quantity of boric acid in water and then adding the $Al_2O_3$ powder. After drying (at 110°C), the respective compacts are produced by means of cold isostatic compression. These specimens are also fired in the Astro furnace under argon.

The results shown in Fig. 8 reveal that the addition of $B_2O_3$ diminishes the densification of $Al_2O_3$ substantially, particularly after firing at 1600°C. Although this influence lessens after firing at 1800°C, it still cannot be ignored. X-ray diffraction analysis fails to detect a new phase in any of the specimens.

### 3.4. Electrical resistance of different composites at room temperature

The electrical resistivity of cylindrical specimens of 30 mm in diameter and 20 mm in height is determined.

To summarize the results for the various specimens after firing at 1700 and 1800°C it can be stated that all

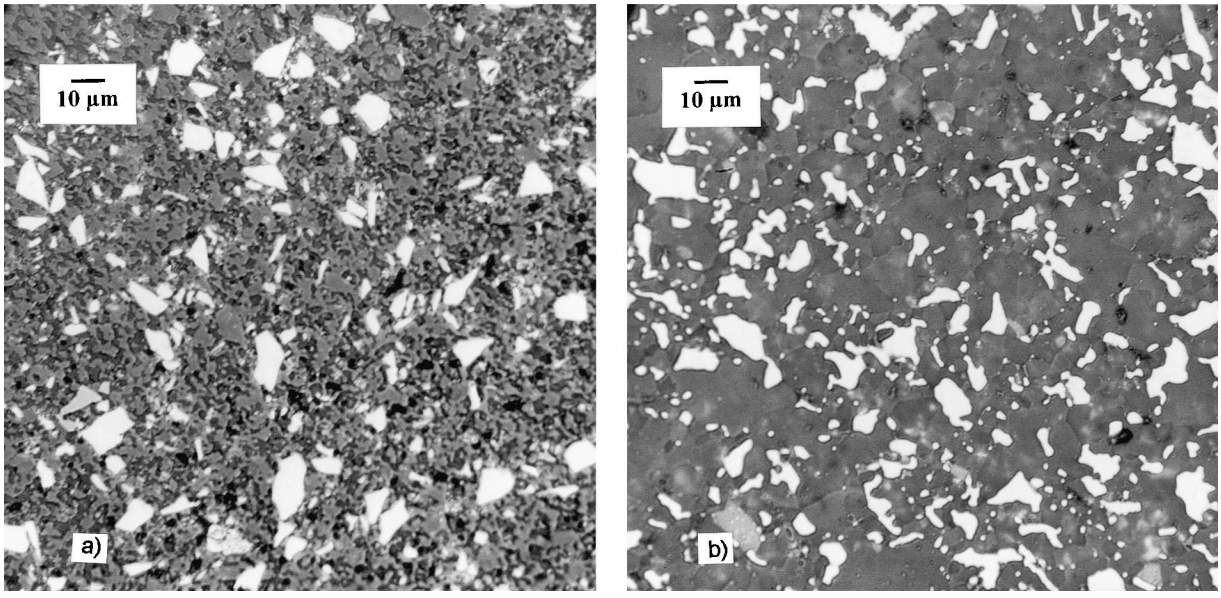


Fig. 5. Optical micrograph of a $Al_2O_3$ composite containing 20 vol% $ZrB_2$ sintered for 1 h at (a) 1600°C, (b) 1800°C (magnification 500×).

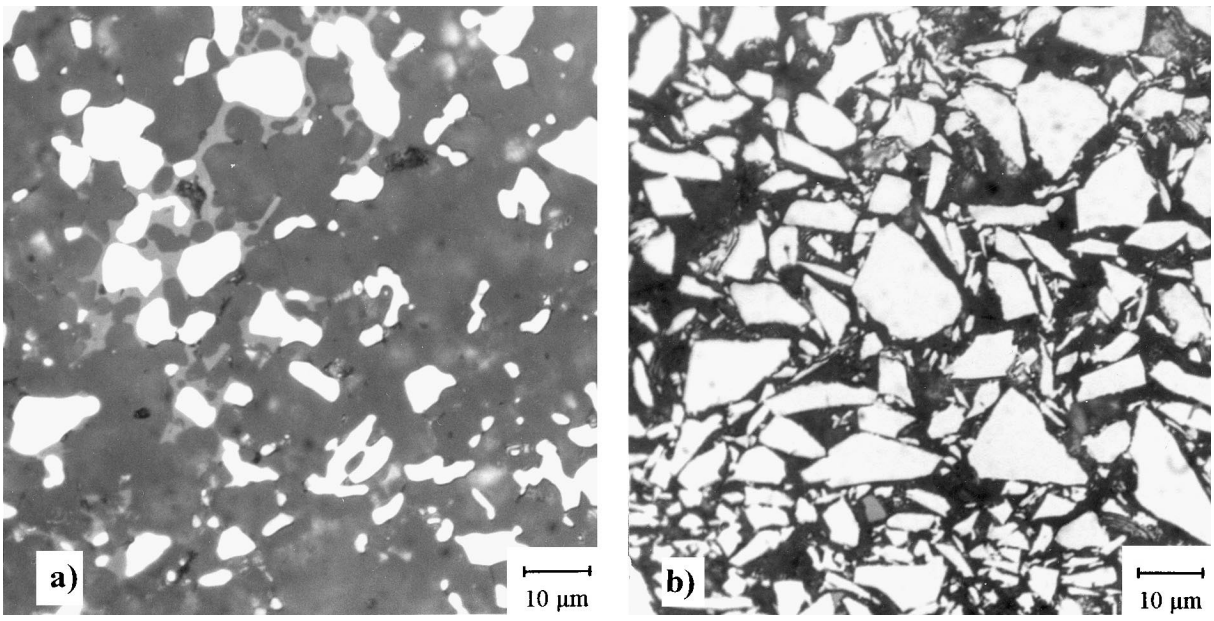


Fig. 6. Optical micrograph of: (a) $Al_2O_3$ containing 20 vol% $ZrB_2$ sintered at 1800°C for 1 h; (b) $ZrB_2$ sintered at 1800°C for 1 h (magnification 1000×).

specimens are revealed to be non-conductors with exception of the composite with 20 vol% $ZrB_2$ sintered at 1800°C. In this case the electrical resistivity is $<0.25$ Ωcm.

## 4. Discussion

As explained in connection with the results of the experiments, Fig. 1 distinguishes between two sintering ranges:

- $T \leqslant 1700$°C
- $T > 1700$°C

These two temperature ranges are discussed separately below.

### 4.1. Sintering at $T \leqslant 1700$°C

A study by Fan and Rahaman examining the zinc oxide–zircon oxide system (ZnO–$ZrO_2$)[4] provides an appropriate comparison. In this study, the influence of the added $ZrO_2$ ($d_{50} = 14$ µm) on the densification behaviour of ZnO was determined at various temperatures. The graph (Fig. 9) below compares a result from this study (influence of various $ZrO_2$ content levels on the relative matrix density of ZnO after firing at 1000°C without a retention period) with the values obtained in the present study in the $Al_2O_3$–$ZrB_2$ system at 1600°C. The temperatures correspond to those at which ZnO and $Al_2O_3$ just attain their highest density. They are thus comparable in terms of kinetics. The influence of the $ZrO_2$ on the sintering behaviour of ZnO is interpreted in the above-stated study as a mechanical impediment, as the inclusion component is chemically inactive in conjunction with the matrix material. According to the cited study, an increase in the $ZrO_2$ content is accompanied by a linear increase in the inclusion component. In the present study, a steep decline in the matrix density is observed with an addition of 2.5 vol% $ZrB_2$, while larger additions result in a linear decline corresponding to the content level (Fig. 9). This indicates that the addition of $ZrB_2$ represents a double impediment:

- even small percentage contents act as chemical impurities
- as percentage contents rise, the mechanical influence predominates

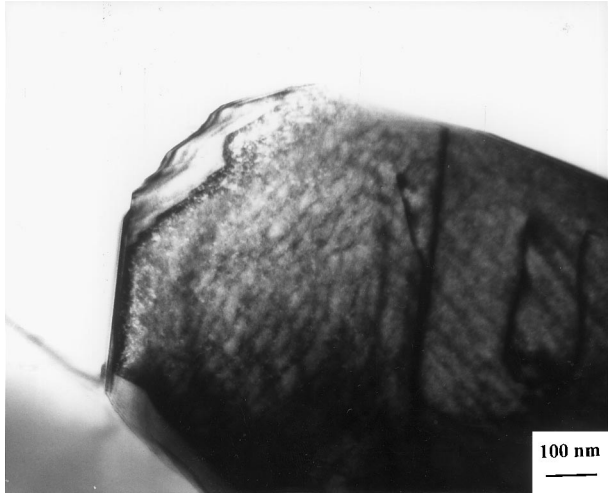


Fig. 7. TEM micrograph of one $ZrB_2$ particle in an $Al_2O_3$ matrix sintered at 1800°C for 1 h.

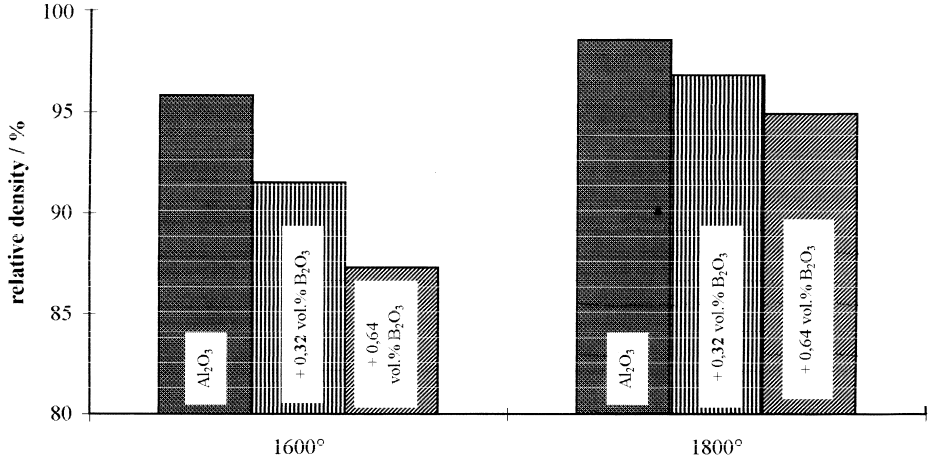


Fig. 8. The influence of $B_2O_3$ on the density of $Al_2O_3$ after firing at 1600 and 1800°C (heating rate: 10 K/min; no soaking time; atmosphere argon).

With an addition of 20 vol% $ZrB_2$, for example, both influencing factors are of roughly the same magnitude at firing temperatures of up to 1600°C (cf. Fig. 9).

Thermochemical equilibrium calculations taking account of the non-ideal behaviour of the $Al_2O_3$–$B_2O_3$ melt phase show that no reactions between $Al_2O_3$ and $ZrB_2$ are to be expected under an argon atmosphere. However, $ZrB_2$ is known to be covered by a layer of $B_2O_3$ of varying thickness; chemisorbed oxygen is certainly present.[5,6] At temperatures above 1000°C, the entire pore volume of the specimen is filled with $B_2O_3$ vapour. In this way, $B_2O_3$ reaches the $Al_2O_3$ surfaces before the densification process begins, and reacts here to form aluminium borate $9Al_2O_3{\cdot}2B_2O_3$ ($A_9B_2$). This behaviour has been confirmed by experimentation.[7]

Although no aluminium borate was detected in the present study, it is known that the very smallest levels of impurity are sufficient to cause substantial interfacial effects. A $B_2O_3$ constituent of 2% by weight in the $ZrB_2$ raw material is sufficient to enable a monomolecular covering of $A_9B_2$ on $Al_2O_3$ in the specimen containing 2.5 vol% $ZrB_2$. The experimental results (Fig. 8) confirm the negative influence of even the most minimal quantities of $B_2O_3$ on the densification behaviour of $Al_2O_3$. It is assumed that the specific free surface energy of the $Al_2O_3$ is reduced as a result of the chemisorption of $B_2O_3$ and its reaction to form aluminium borate, and that the resultant reduced driving force leads to the observed reduction in the sintering rate. This explanation is supported by the established fact that $A_9B_2$ is difficult to sinter.[8]

In addition to the chemical influence, the rising percentage contents of $ZrB_2$ also increasingly inhibit densification. This brings us to Lange's model to describe sintering kinetics.[9] Lange's studies reveal that the extent of densification is dependent to a decisive degree on the distances between the particles. When using this model to evaluate the results of the present experiments, the

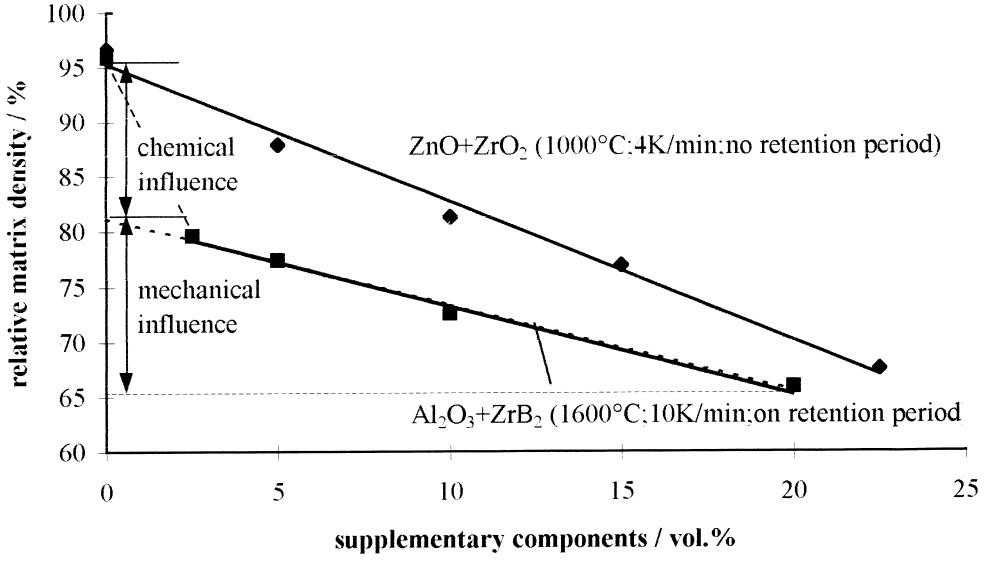


Fig. 9. Density of various $Al_2O_3$–$ZrB_2$ composites at 1600°C in comparison to values stated in a study of the ZnO–$ZrO_2$ system at 1000°C.[4]

observed interfacial effect of the impurity is to be taken into account, i.e. deducted from the initial value (0% $ZrB_2$).

To this end, isothermic sections are applied in Fig. 1 at $T \leqslant 1700°C$, and the linear approximated mechanical influence of $ZrB_2$ is extrapolated down to a concentration of 0%. On the basis of the resultant corrected shrinkage of the matrix without an added component (0% $ZrB_2$), the calculation according to Lange is then performed as follows:

$$\rho_{mc} = \frac{\rho_{mco}}{\left[1 - \left(1 - \frac{\rho_0}{\rho_m}\right)^{1/3}\left(1 - \left(\frac{1}{\alpha}\right)\left(\frac{f}{s}\right)^{1/3}\right)\right]^3} \quad (4)$$

whereby

$\rho_{mc}$ = matrix density of composite in g/cm$^3$
$\rho_{mco}$ = matrix green density of composite in g/cm$^3$
$\rho_0$ = green density of matrix without additive in g/cm$^3$
$\rho_m$ = density of matrix without additive in g/cm$^3$
$\alpha$ = constant

$f$ is the percentage volume of the inclusion phase, and is calculated as follows

$$f = F(\rho_{c0}/\rho_{tc}) \quad (5)$$

whereby

$\rho_{c0}$ = green density of composite in g/cm$^3$
$\rho_{tc}$ = theoretical density of composite in g/cm$^3$
$F$ = percentage volume of inclusion phase at 0% porosity.

In accordance with Lange's results, a value of 0.16 is employed for $s$. This value correspond to the percentage volume at which the included particles just come into contact with one another.[9] $\alpha$ is a constant which the model defines as being dependent on the selected unit cell. The results for the various percentage contents of $ZrB_2$ are shown in Fig. 10, and reveal a good match between theoretical and practical assessment.

This approximation is attained for the specimens containing 2.5, 5 and 10 vol% $ZrB_2$ via $\alpha$ values which are greater than those used by Lange (Fig. 11). Lange also establishes in the ZnO–SiC system that the optimum $\alpha$ values decrease as the inclusion volumes increase. The reduction accompanying increasing particle density can be explained in geometric terms by the fact that the unit cell on which the calculation is based becomes increasingly more simple and attains a virtually cubic primitive form at $\alpha = 2.1$ (for 20 vol% $ZrB_2$) (body diagonal = $a_0\ 3^{1/2}$).

This correlation (Fig. 11) closely approximates a power function:

$$\alpha = 16.2^*(\%\text{vol.}ZrB_2)^{-2/3}. \quad (6)$$

With the aid of this result it is now possible to model the densification of $Al_2O_3$–$ZrB_2$ composites, which is of practical interest.

### 4.2. Sintering at T > 1700°C

As the sintering experiments show, the densification process is accelerated above 1700°C. The matrix sintering rate of the specimen containing 20 vol% $ZrB_2$ far exceeds the rate of pure $Al_2O_3$ (Fig. 3). The sintering mechanism has evidently altered as a result of the formation of a liquid phase. Pronounced melt phase pools are recognisable in the microstructure of the specimen containing 20 vol% $ZrB_2$ (1800°C/1 h) (Fig. 6a). The melt, which is proven to consist primarily of the elements aluminium, boron and oxygen, is situated both between $Al_2O_3$ particles and between $Al_2O_3$ and $ZrB_2$

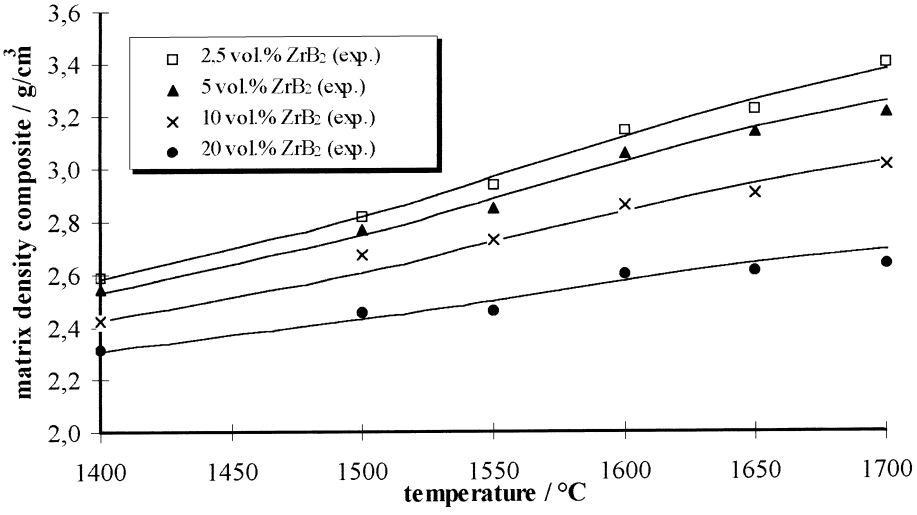


Fig. 10. Comparison of experimental values and calculated values (lines) for $Al_2O_3 + ZrB_2$ (s = 0.16).

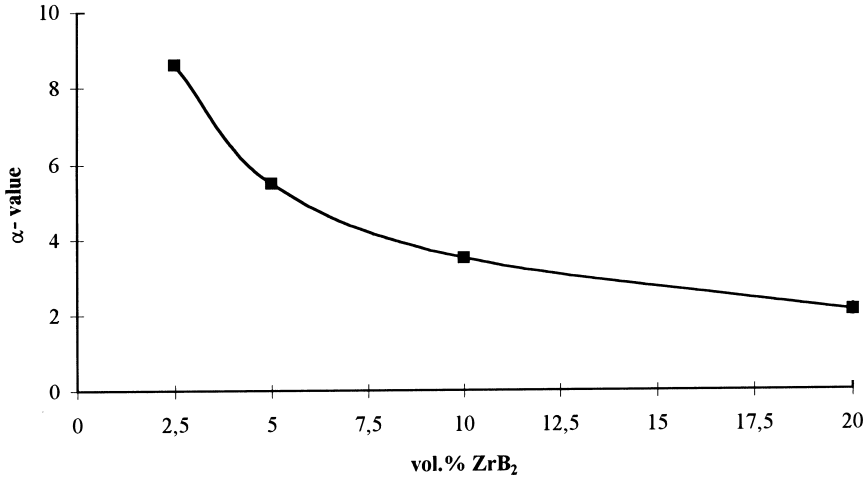


Fig. 11. Employed α-values as a function of the percentage volume of $ZrB_2$.

particles. The following equations thus apply for the specific free interfacial energies between the phases:

$$2\gamma_{Al_2O_3;liquid} < \gamma_{Al_2O_3;Al_2O_3} \quad (7)$$

and

$$\gamma_{Al_2O_3;liquid} + \gamma_{ZrB_2;liquid} < \gamma_{Al_2O_3;ZrB_2} \quad (8)$$

Good or complete wettability of the solid phases by the liquid phases is an elementary precondition for liquid phase sintering.[10] The specimens undergo the following sintering process.

In a temperature interval from 1700 to 1750°C, the aluminium borate phase which has formed at lower temperatures on the free $Al_2O_3$ surfaces (see above) melts. A particle rearrangement process first takes place, i.e. the $Al_2O_3$ grains rebound from one another as a result of capillary forces and form a denser packing.[10] This process is particularly pronounced in the specimen containing 20 vol% $ZrB_2$, as the microstructure here initially possesses the highest open porosity, which then swiftly disappears. The $ZrB_2$ particles are also involved in this rearrangement process, thus increasing their mutual contact. In contrast, the microstructures of the other specimens are already denser upon reaching 1700°C, providing a poor basis for an effective rearrangement process by the liquid phase. The particle rearrangement process is followed by a process of dissolution and renewed crystallisation, for which purpose $Al_2O_3$ must be dissoluble in the melt phase. As a result, the porosity falls and the microstructure becomes coarser. As soon as the liquid phase has been consumed, further densification takes place by means of a purely solid phase reaction process.

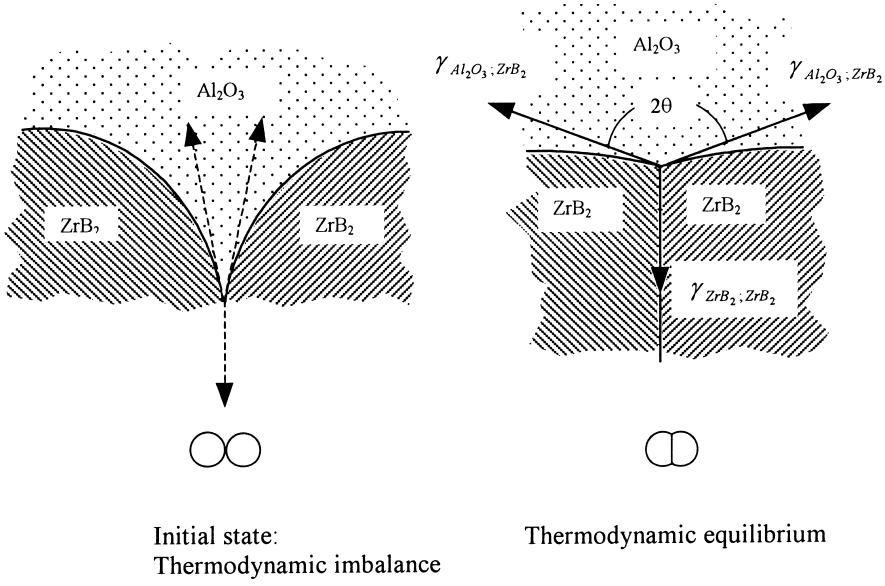


Fig. 12. Boundary phase equilibruium in the $Al_2O_3$–$ZrB_2$ system.

### 4.3. Microstructure

The shape of the $ZrB_2$ particles changes substantially (Figs. 5b and 6a), whereby they strive to attain a minimum surface-to-volume energy ratio:

$$V\Delta g_V + \Sigma F_{hkl}\gamma_{hkl} = \text{Min} \quad (9)$$

whereby

$V$ = volume of crystal
$\Delta g_V$ = specific free Gibbs energy of crystal volume
$F_{hki}$ = sum of surfaces of orientation hkl
$\gamma_{hkl}$ = specific free surface energy.

Energy minimisation is effected via the formation of microscopically fine steps consisting of (low-energy) faces of the equilibrium shape (cf. Fig. 7). The resultant macroscopic form is that of a rounded crystal.[11]

In addition to rounding, the $ZrB_2$ particles also undergo coalescence in the $Al_2O_3$ matrix. In the specimen containing 20 vol% $ZrB_2$, this results in a penetration structure which possesses good electrical conductivity.

The particles' tendency to coalesce is dependent on the interfacial tension. The following equilibrium relation applies for the case under consideration here, which is illustrated in diagram form in Fig. 12:

$$\gamma_{ZrB_2;ZrB_2} = 2\gamma_{ZrB_2;Al_2O_3}\cos\theta \quad (10)$$

As the particles coalesce, the following relation applies:

$$\gamma_{ZrB_2;ZrB_2} \ll \gamma_{ZrB_2;Al_2O_3} \quad (11)$$

i.e. the dihedral equilibrium angle is $>60°$.

It is revealed that the strong coalescence of the $ZrB_2$ particles in the $Al_2O_3$ matrix is initiated by the high phase boundary energy, $\gamma_{Al_2O_3;ZrB_2}$ ($\theta > 60°$). This is accountable to the different lattice bonds of the two phases. $Al_2O_3$ possesses an ionic bond constituent of 45–50%,[12] while $ZrB_2$ is characterised by a high metallic bond content.[13] However pure $ZrB_2$ does not sinter at 1800°C (cf. Fig. 6b).

## 5. Summary

The experiments show that the pressureless sintering of $Al_2O_3$ containing $ZrB_2$ can be divided into two characteristic temperature ranges. At temperatures $\leqslant$1700°C, the added hard material severely impedes the densification process. This is due to the fact that even the most minimal $B_2O_3$ impurities in the $ZrB_2$ are chemisorbed onto the $Al_2O_3$ surfaces prior to the commencement of the sintering process, and lead to the formation of aluminium borate, as a result of which the level of sintering activity drops. The established mechanical influence of chemically inert particles — in this case $ZrB_2$ — also takes effect, as is described by Lange's model, for example. In the present case this model enables the density development of composite materials in the $Al_2O_3$–$ZrB_2$ system to be predicted on the basis of a small number of experiments.

At temperatures >1700°C, the specimen containing 20 vol% $ZrB_2$ in particular undergoes a very rapid increase in density. This activated sintering process is due to the formation of an aluminium borate melt. As a result, all the specimens attain matrix densities greater than 95% of the theoretical density after firing at 1800°C and a soaking time of 30 min. The negative influence of increasing inclusion volumes on the relative density almost completely disappears in this temperature range. At these high temperatures, the $ZrB_2$ particles change in shape, resulting in the macroscopic appearance of rounded crystals. They are also subject to pronounced coalescence, initiated by the high phase boundary energy, $\gamma_{Al_2O_3;ZrB_2}$.

The results of this study show that dense composites can be produced in the $Al_2O_3$–$ZrB_2$ system. On the basis of the combination of high densities and the inclusion components, outstandingly good mechanical, thermomechanical and electrical characteristics are to be expected. Cost-effective production by means of pressureless sintering provides broad potential for technical applications.

## Acknowledgements

The work was initiated by Dr. T. Rymon-Lipinski and financially supported by Dr. C. Otto Feuerfest GmbH, for which we thank him. Professor Dr. R. Telle, RWTH Aachen, we thank him for his valuable references to the evaluation of the results. We thank Dr. A. Boccaccini and Dr. F. Brunk for their assistance in the discussion of sinter kinetics.

## References

1. Sudre, O. and Lange, F. F., Effect of inclusions on densification: I, microstructural development in an $Al_2O_3$ matrix containing a high volume fraction of $ZrO_2$ inclusions. *Journal of the American Ceramic Society*, 1992, **75**, 519–524.
2. Powell, C. F., Borides. In *High Temperature Materials and Technology*, ed. I. E. Campbell and E. M. Sherwood. John Wiley & Sons, Inc., New York, 1967.
3. Rahaman, M. N. and De Jonghe, L. C., Effect of rigid inclusions on the sintering of glass powder compacts. *Journal of the American Ceramic Society*, 1987, **70**, C-348–C-351.
4. Fan, C. -L. and Rahaman, M. N., Factors controlling the sintering of ceramic particulate composites: I, conventional processing. *Journal of the American Ceramic Society*, 1992, **75**, 2056–2065.
5. Zdaniewski, W. A. and Brungard, N. L., X-ray photoelectron spectroscopy studies of metallic diborides. *Journal of the American Ceramic Society*, 1992, **75**, 2849–2856.

6. Klinger, H. and Telle, R., Herstellung von mehrphasigen Hartstoffen im System $B_4C$–Si–Ti durch reaktive Schmelzinfiltration, Sprechsaal. *Ceramics & Materials*, 1995, **128**, 11–15.
7. Misirli, Z., Erkalfa, H. and Özkan, O. T., Effect of $B_2O_3$ addition on the sintering of $\alpha$-$Al_2O_3$. *Ceramics International*, 1996, **22**, 33–37.
8. Ray, S. P., Preparation and characterization of aluminium borate. *Journal of the American Ceramic Society*, 1992, **75**, 2605–2609.
9. Lange, F. F., Constrained network model for predicting densification behavior of composite powders. *Journal Materials Research*, 1987, **2**, 59–65.
10. Schatt, W., *Sintervorgänge*. VDI Verlag, Düsseldorf, 1992.
11. Stranski, I. N., Eine Plauderei über Gleichgewichtsformen von Kristallen. *Journal of Crystal Growth*, 1972, 3–8.
12. Petzold, A., Ulbricht, J., *Aluminiumoxid, Rohstoff-Werkstoff-Werkstoffkomponente*. Deutscher Verlag für Grundstoffindustrie, Leipzig, 1991.
13. Telle, R., Boride and carbide ceramics. In *Materials Science and Technology, A Comprehensive Treatment*, Vol. 11, ed. R. W. Cahn, P. Haasen, E. J. Kramer, *Structure and Properties of Ceramics*, Ed. M. V. Swain. VCH Verlagsgesellschaft Weinheim, 1994.